Numerical Investigation of Non-Fourier Flux Theory with Chemical Action on Maxwell Radiating Nanoliquid: A Biomedical Application

Suneetha Sangapatnam, Subbarayudu Ketineni, Ali J. Chamkha, and Bala Anki Reddy Polu

Abstract In the modern critique, we deliberated a theoretical model of blood with carbon nanotubes (CNT's)—ejected in a Maxwell fluid with dissipative nanoparticles through binary chemical reaction lying on a stretching sheet by means of aligned field of magnetism. A customized Arrhenius function is imposed for energy activation. A non-linear radiation and a heat source/sink which is not uniform are incorporated in the energy equation which named as Cattaneo–Christov model of heat diffusion. Convective slip and suction are also added. Single and multiple walled nanotubes of carbon are employed with human blood as working liquid. A non-linear system is obtained for the considered problem, and an attempt is made by using Runge–Kutta fourth order through shooting (RK4S) method—bvp4c codes in MATLAB. The results are discussed and plotted in graphs for embedded parameters of concern. Higher activation energy improves the concentration, and a rise in chemical reaction rate constant raises Sherwood number. This study is thoughtful for medical surgeons during surgery in regulating the blood flow.

Keywords Cattaneo–Christov heat flux · SWCNT and MWCNT's · Activation energy · Binary chemical reaction · Human blood · Non-uniform heat source/sink

Nomenclature

g'	Acceleration due to gravity
T_∞	Ambient fluid temperature
T_f	Hot fluid temperature

S. Sangapatnam (✉) · S. Ketineni
Department of Applied Mathematics, Yogi Vemana University, Kadapa 516005, India
e-mail: suneethayvu@gmail.com

A. J. Chamkha
Mechanical Engineering Department, Prince Mohammad Endowment for Nanoscience and Technology, Prince Mohammad Bin Fahd University, Al-Khobar 31952, Saudi Arabia

B. A. R. Polu
Department of Mathematics, School of Advanced Sciences, VIT, Vellore 632014, India

B. Rushi Kumar et al. (eds.), *Advances in Fluid Dynamics*, Lecture Notes in Mechanical Engineering, https://doi.org/10.1007/978-981-15-4308-1_61

h_f	Convective heat transfer coefficient
Ec	Eckert number
M	Magnetic parameter
E	Non-dimensional activation energy
Pr	Prandtl number
$\lambda*$	Thermal buoyancy parameter
Nr	Solutal buoyancy parameter
q_r	Radiative heat flux
Sc	Schmidt number
S	Suction/injection parameter
T	Temperature
$\bar{k}_{\text{CNT}}$	Thermal conductivities of CNT's
$\bar{k}_f$	Thermal conductivity of the host fluid
$\bar{k}_{\text{nf}}$	Thermal conductivity of the nanofluid
Rd	Radiation parameter
B_0	Uniform magnetic field strength
U_w	Velocity at wall
u	Velocity component along the x-axis
v	Velocity component along y-axis
A	Velocity slip factor
v_w	Wall mass flux
T_w	Wall temperature
C_w	Wall concentrate
Σ	Non-dimensional chemical reaction rate constant
θ_w	Temperature ratio parameter
μ_f	Fluid viscosity
μ_{nf}	Nanofluid viscosity
χ	Nanoparticles fraction
ρ_f	Fluid density
ρ_{CNT}	Thermal conductivities of CNT's
$(\rho C_p)_f$	Fluid heat capacitance
$(\rho C_p)_{\text{nf}}$	Nanofluid heat capacitance
$(\rho C_p)_{\text{CNT}}$	CNT's heat capacity
ρ_{nf}	Density of the nanofluid
$\sigma**$	Electric conductivity
α_{nf}	Thermal diffusivity of nanofluids
ξ	Aligned magnetic field parameter

1 Introduction

With the enormous awareness of current engineering technology, a new material known as nanomaterial that had got extensive enactment in fields like industry, biomedicine, electronics and transportation [1]. Nanofluid is a fluid having nano-sized metallic or non-metallic particles. Carbon atoms are arranged in empty cylindrical forms which are known as Carbon nanotubes, and the walls are in hexagonal shape of graphite. Furthermore, depending upon the number of graphene sheets rolled concentrically, single-wall and multi-wall carbon nanotubes are prepared. Fluid mechanics is the branch of physics concerned with the mechanics of fluids which are in movement. Here, blood is treated as a liquid that helps the bioengineers to model an upgraded synthetic organ and discovering remedies related to the human body diseases. Fourier did the introductory work for describing the flow temperature in parabolic equations and got a negative feature which discloses a small interruption throughout the medium. So, several investigators make an effort to alter the classical Fourier's law. Among them, Cattaneo [2] was one who productively modified the law by attaching the heat relaxation time which let the movement of heat by the employment of transmission of heat waves with unchanging speed. Christov [3] renovated the Maxwell–Cattaneo law with time derivative to get material invariance. Bala Anki Reddy and Suneetha [4] disclosed the fluid temperature and the heat relaxation time which are encountered in nature. Kolin [5] was the first person who has given the concept of electromagnetic fields in medical research. A force branded as Lorentz force has been generated by both magnetic and electric fields which has empathy to oppose the motion of the liquid (blood). By applying external magnetic field, the diseases like cardiovascular, haemorrhages and hypertension can be treated and have many real applications such as MRI, cancer therapy. Some authors [6, 7] suggested that when a human system is rendered to a magnetic flux externally, it starts to slow down the blood flow. The impact of radiation on blood flow has many uses in medical treatment methods. With the help of electromagnetic radiation, oncologist treats the cancerous tissues (Szasz [8]) by overheating them. Many investigators [9–11] explored the characteristics of non-Newtonian fluids where the heat radiation is not linear. Non-linear radiation is apt for peak and small temperature variations of surface and the fluid far from the surface. MHD flow over a stretching surface with Maxwell nanofluid was numerically explained by Reddy et al. [12]. Blood flow through a vessel with slip velocity near the wall was developed by Misra and Kar [13]. Gebhart [14] was first who revealed the significance of dissipation in convection. The process in which a part of kinetic energy converts into thermal energy by the viscosity of the fluid in motion is an irreversible process known as viscous dissipation. Reddy et al. [15] conducted a numerical experiment on the magneto-hydrodynamic flow of blood over a porous inclined plate with dissipation. By generating heat in the fluid mass, the temperature circulation can be changed which affects the rate of particle deposition. At present, we consider source/sink of heat which is not uniform. Some related studies on this were carried out by several investigators [16–20]. Svante Arrhenius was the first person who proposed the term activation energy in 1889. He narrated

it as the least energy required to start the reaction. In 1990, Bestman [21] disclosed binary chemical reaction in a fluid flow. An equation which describes the association with the activation energy and the reaction rate is referred as the Arrhenius equation. The Arrhenius equation is $K = B_1(T - T_\infty)^m \, \mathrm{e}^{\left(\frac{-E_a}{k(T-T_\infty)}\right)}$ where K—reaction rate, B_1—exponential factor, E_a—the activation energy, T—temperature of the fluid and $k = 8.61 \times 10^{-5}$ eV/K is the Boltzmann constant. Actually, when temperature rises regularly, the rate of reaction rises. A reaction that occurs in two steps which is familiar in both (liquid and vapour) deposition processes is known as a binary chemical reaction, and some of its applications are varnishing of metallic objects and manufacturing of electronic tools investigated by Shafique et al. [22]. Few existing reviews aforementioned topic is revealed in Refs. [23, 24]. The literature survey shows that there are many investigations done on nanofluids with C-CHF model on stretching plane. Still there is no work has been explored to discuss the aligned magneto-radiating fluid on blood. To fill the gap in this regard, current attempt is done to analyze the effect on aligned magneto-hydrodynamic 2D Maxwell nanofluid with CNT's on blood flow past a stretching sheet with non-linear heat radiation of non-Fourier flux theory. The specific attention of the present effort is to inspect the comparable solutions of the non-linear partial differential equations for some values of the parameters by using the shooting method.

2 Description of the Problem

Let us consider the Maxwell nanofluid past a stretchable plane with blood flow. In this autopsy, SWCNT's and MWCNT's are used. The physical characteristics of the host fluid and CNT's are drafted in Table 1. In this autopsy, Cattaneo—Christov heat flux model (C-CHFM) is considered. The primary fluid is taken as blood which is viscous in nature. The problem is characterized under the action of viscous dissipation, activation energy, binary chemical reaction, thermal radiation which is not linear, non-uniform heat source/sink and aligned magnetic field. Sheet stretches in the route of x-axis and erects to the y-axis. The magnetic flux B is employed vertically to the sheet. The stimulated magnetic field is tiny as a result a very minute Reynolds number exist. $U_w(x) = cx$ $(c > 0)$ be the velocity along the stretching direction. Temperature is synchronized by convection and depicted in

Table 1 Thermo-physical characteristics of base fluids and CNTs [25]

Physical properties	Host fluid (human blood)	Nanoparticles	
		SWCNT	MWCNT
C_p	3594	425	796
ρ	1053	2600	1600
κ	0.492	6600	3000
$\beta \times 10^{-5}$	0.18	2.6	2.8

Fig. 1 Flow framework

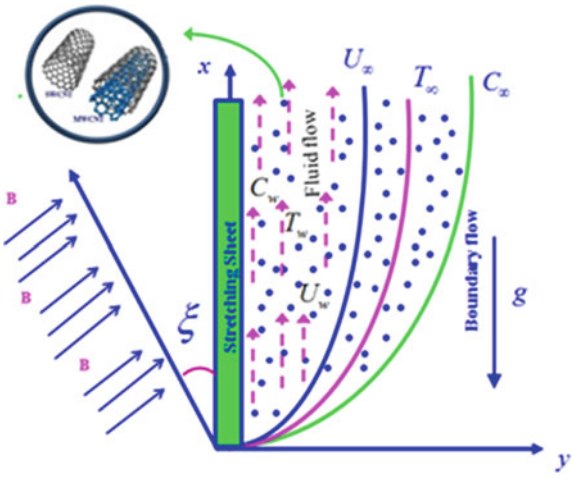

Fig. 1. The flow under these attentions can be put into the ensuing form:

$$\partial_x u + \partial_y v = 0 \tag{1}$$

$$u\,(\,\partial_x u) + \lambda_1\big(u^2(\partial_{xx} u) + v^2(\partial_{yy} u) + 2uv(\partial_{xy} u)\big) + v(\partial_y u) = \frac{1}{\rho_{\mathrm{nf}}}\big(\mu_{\mathrm{nf}}(\partial_{yy} u) + (\rho\beta)_f g'(T - T_\infty) - (\rho\beta^*)_f g'(C - C_\infty) - \sin^2 \xi \sigma B_0^2(x) u\big) \tag{2}$$

$$\big(\rho C_p\big)_{\mathrm{nf}}\big(u\,(\partial_x T) + v\,(\partial_y T)\big) = -\nabla \cdot q_0 - \frac{1}{\upsilon}\big(\partial_y q_r\big) + \frac{\upsilon}{c_p}\big(\partial_y u\big)^2 + q''' \tag{3}$$

$$u(\partial_x C) + v\big(\partial_y C\big) = D\big(\partial_{yy} C\big) - k_r^2\left(\frac{T}{T_\infty}\right)^m (C - C_\infty) e^{-\frac{E_a}{kT}} \tag{4}$$

The expression $k_r^2\left(\frac{T}{T_\infty}\right)^m e^{-\frac{E_a}{kT}}$ in Eq. (4) designates the modified Arrhenius equation, reaction rate—k_r^2, the fixed rate constants—m, $-1 < m < 1$.

The C-CHF is expressed as

$$q_0 + \lambda^*\big(\partial_t q_0 + V' \cdot \nabla q_0 - q_0 \cdot \nabla V' + \big(\nabla \cdot V'\big) q_0\big) = -\overline{k}_f(\nabla \cdot T) \tag{5}$$

where λ^*—flux relaxation time and V'—velocity vector. Equation (5) is transformed into Fourier's law for $\lambda^* = 0$, $\nabla . V' = 0$, and for incompressible fluid, Eq. (5) receipts the outline

$$q_0 + \lambda^*\big(\partial_t q_0 + V' \cdot \nabla q_0 - q_0 \cdot \nabla V'\big) = -\overline{k}_f\,(\nabla \cdot T\,) \tag{6}$$

The energy equation after eliminating q_0 from Eqs. (3) and (6) is

$$u(\partial_x T) + \lambda^*\Big(\big(u(\partial_x T) + v\big(\partial_y T\big)\big)^2 + u\big((\partial_x u)(\partial_x T) + (\partial_x v)\big(\partial_y T\big)\big) + v\big((\partial_y v)\big(\partial_y T\big) + \big(\partial_y u\big)(\partial_x T)\big)\Big) + v\big(\partial_y T\big) = \alpha_{\mathrm{nf}}\big(\partial_{yy} T\big) - \frac{1}{\upsilon}\big(\partial_y q_r\big) + \frac{\upsilon}{c_p}\big(\partial_y u\big)^2 + q''' \tag{7}$$

The non-uniform source/sink of heat q''' is modelled as

$$q''' = \frac{kU_w}{x\upsilon}\big[A * (T_w - T_\infty) f' + B * (T - T_\infty)\big]$$

where A^* and B^* denote the space- and temperature-dependent coefficients. For $A^* > 0$ and $B^* > 0$, internally heat is generated, and for $A^* < 0$, $B^* < 0$, heat is absorbed internally.

The heat flux q_r is given by means of the Rosseland approximation

$$q_r = -\left(\frac{4}{3\,K^*}\right)\mathrm{grad}(\sigma^* T^4) \tag{8}$$

where K^*—the absorption coefficient, e_b—the emission from a blackbody and $\sigma^* = 5.6697 \times 10^{-8}\ \mathrm{Wm^{-2}\,K^{-4}}$ be the Stefan–Boltzmann constant.

The term T^4 is a function of temperature and can be extended as Taylor series in terms of T_∞ and estimated by ignoring terms with higher order.

$$T^4 = T_\infty^4\{1 + (\theta_w - 1)\theta\}^4 \tag{9}$$

where $\theta_w = \frac{T_w}{T_\infty}$, $\theta_w > 1$ be the wall temperature ratio parameter.

Xue launched a model which depends on Maxwell theory and reimburses the effect of the space distribution on CNT's. In this paper, Xue model is used as follows:

$$\frac{\bar{k}_{\mathrm{nf}}}{\bar{k}_f} = \frac{1 - \chi + 2\chi\left(\frac{\bar{k}_{\mathrm{CNT}}}{\bar{k}_{\mathrm{CNT}} - \bar{k}_f}\right)\ \log\frac{\bar{k}_{\mathrm{CNT}} + \bar{k}_f}{2\bar{k}_f}}{1 - \chi + 2\chi\left(\frac{\bar{k}_f}{\bar{k}_{\mathrm{CNT}} - \bar{k}_f}\right)\ \log\frac{\bar{k}_{\mathrm{CNT}} + \bar{k}_f}{2\bar{k}_f}} \tag{10}$$

which is interpreted as:

$$\left.\begin{aligned} \frac{\rho_{\mathrm{nf}}}{\rho_f} = (1 - \chi) + \frac{\chi\rho_{\mathrm{CNT}}}{\rho_f}\ ,\ \frac{\big(\rho C_p\big)_{\mathrm{nf}}}{\big(\rho C_p\big)_f} = (1 - \chi) + \frac{\chi\big(\rho C_p\big)_{\mathrm{CNT}}}{\big(\rho C_p\big)_f} \\ \mu_{\mathrm{nf}} = (\upsilon\rho)_{\mathrm{nf}},\ \ \mu_{\mathrm{nf}} = \mu_f\,(1 - \chi)^{-2.5}\ ,\ \bar{k}_{\mathrm{nf}} = \big(\alpha\big(\rho C_p\big)\big)_{\mathrm{nf}} \end{aligned}\right\} \tag{11}$$

and undergoes the boundary conditions:

$$y = 0 : u = U_w(x) + A\left(\partial_y u\right),\ v = -v_w,\ -k\left(\partial_y T\right) = h_f(T_f - T),\ C = C_w$$

$$y \to \infty : u \to 0\ ,\ T \to T_\infty\ ,\ C \to C_\infty \tag{12}$$

Using the similarity transformations,

$$\eta = \sqrt{\frac{c}{v}}\, y,\ \psi(x, y) = \sqrt{cv}\, x f(\eta), \quad \theta(\eta) = \frac{T - T_\infty}{T_w - T_\infty},\quad \phi(\eta) = \frac{C - C_\infty}{C_w - C_\infty}$$
$$u = cx f'(\eta),\ v = -\sqrt{cv}\, f(\eta) \tag{13}$$

Adopting Eqs. (10, 11, 13) in Eqs. (1, 2, 7, 4), we have

$$d_{\eta\eta\eta} f + (1-\chi)^{2.5}\left\{\left(1 - \chi + \chi\frac{(\rho\beta)_{\mathrm{CNT}}}{(\rho\beta)_f}\right)(\lambda\theta - Nr\phi) - \sin^2\xi M^2\left(d_\eta f\right)\right\}$$
$$-(1-\chi)^{2.5}\left(1 - \chi + \chi\frac{\rho_{\mathrm{CNT}}}{\rho_f}\right)\left\{\left(d_\eta f\right)^2 - f\left(d_{\eta\eta} f\right)\right.$$
$$\left.+\alpha\left(f^2\left(d_{\eta\eta\eta} f\right) - 2f\left(d_\eta f\right)\left(d_{\eta\eta} f\right)\right)\right\} = 0 \tag{14}$$

$$\frac{1}{\mathrm{Pr}}\left\{\left(d_{\eta\eta}\theta\right)\left\{\frac{k_{\mathrm{nf}}}{k_f} + \frac{4}{3}\mathrm{Rd}[(\theta_w - 1)\theta + 1]^3\right\} + 4\mathrm{Rd}[(\theta_w - 1)\theta + 1]^2(\theta_w - 1)\left(d_\eta\theta\right)^2\right\}$$
$$+\left\{1 - \chi + \chi\frac{(\rho c_p)_{\mathrm{CNT}}}{(\rho c_p)_f}\right\}\left\{f\left(d_\eta\theta\right) - \gamma\left(f\left(d_\eta f\right)\left(d_\eta\theta\right) + f^2\left(d_{\eta\eta}\theta\right)\right)\right\}$$
$$+\mathrm{Ec}\left(d_{\eta\eta} f\right) + A * \left(d_\eta f\right) + B * \theta = 0 \tag{15}$$

$$d_{\eta\eta}\phi + \mathrm{Sc}\ f\ (d_\eta\phi) - \ \mathrm{Sc}\ \sigma\ \phi\ [\theta(\theta_w - 1) + 1]^m e^{-\ \frac{E}{\theta(\theta_w - 1) + 1}} = 0 \tag{16}$$

Together with the boundary conditions

$$f(\eta) = S,\ d_\eta f(\eta) = 1 + \delta\, d_{\eta\eta} f(0),\ d_\eta\theta(\eta) = -Bi(1 - \theta(\eta)), \phi\,(\eta) = 1 \text{ at } \eta = 0,$$
$$d_\eta f(\eta) = 0,\ \ \theta(\eta) = 0\,,\ \ \phi(\eta) = 0\ \ \text{at } \eta = 0 \text{ at } \eta \to \infty \tag{17}$$

where

$$\mathrm{Sc} = \frac{\upsilon}{D},\ \ \sigma = \frac{k_r^2}{c},\ \ E = \frac{E_a}{kT_\infty},\ \ \lambda = \frac{\mathrm{Gr}_x}{\mathrm{Re}_x^2},\ \ \mathrm{Gr}_x = \frac{(\rho\beta)_f g'(T_w - T_\infty)x^3}{\upsilon^2\rho_f},$$
$$Nr = \frac{\mathrm{Gc}_x}{\mathrm{Re}_x^2}, \mathrm{Gc}_x = \frac{(\rho\beta^*)_f g'(C_w - C_\infty)x^3}{\upsilon^2\rho_f},\ \ \mathrm{Re}_x^2 = \frac{U_w^2 x^2}{\upsilon^2}, M = B_0\sqrt{\frac{\sigma}{a\rho_f}}\,x,$$
$$\alpha = \lambda_1 c,\ \ \gamma = \lambda^* c, \mathrm{Rd} = \frac{4\sigma^* T_\infty^{*^3}}{kk_1},\ \ \mathrm{Ec} = \frac{U_w^2}{C_p(T_w - T_\infty)},\ \ \mathrm{Pr} = \frac{\left(\mu C_p\right)_f}{k},$$
$$S = \frac{v_w}{a\upsilon_f},\ \ \delta = A\sqrt{\frac{c}{\upsilon}},\ \ Bi = \left(\frac{h_f}{\overline{k}_f}\right)\sqrt{\upsilon_f/c}$$

3 Quantities of Interest

The quantities of interest for considering flow are surface drag force, local Nusselt number and Sherwood number, which are as follows:

$$C_{f_x} = \frac{\tau_w}{\rho_f U_w^2},\quad Nu_x = \frac{xq_w}{\overline{k}_f(T_w - T_\infty)} \text{ and } \mathrm{Sh}_x = \frac{xq_m}{D(C_w - C_\infty)} \tag{18}$$

where τ_w(skin friction of the wall), q_w(heat flux of the wall) and q_m(mass flux of the wall) which are specified as

$$\tau_w = \mu_{\mathrm{nf}}\left(\partial_y u\right)_{y=0},\ q_w = -x\overline{k}_{\mathrm{nf}}\left(\partial_y T\right)_{y=0} + \left(q_r\right)_{y=0} \text{ and } q_m = -D\left(\partial_y C\right)_{y=0} \tag{19}$$

In view of Eqs. (18) and (19), the dimensionless surface drag force, local Nusselt number and local Sherwood number are given by

$$C_f \mathrm{Re}_x^{1/2} = \frac{1}{(1-\chi)^{2.5}}\left(d_{\eta\eta} f(0)\right),$$
$$Nu_x \mathrm{Re}_x^{-1/2} = -\left\{\frac{\overline{k}_{\mathrm{nf}}}{\overline{k}_f} + \frac{4}{3}\mathrm{Rd}[(\theta_w - 1)\theta(0) + 1]^3\right\}\left(d_\eta\theta(0)\right)$$
$$\text{and } \mathrm{Sh}_x \mathrm{Re}_x^{-1/2} = -d_\eta\phi(0), \tag{20}$$

wherever $\mathrm{Re}_x = \frac{U_w x}{\upsilon}$ signifies Reynolds number.

4 Results and Discussion

Blood flow (host fluid) of MHD-based CNT's on C-CHFM with non-linear radiant heat along with binary chemical changes on Maxwell nanofluid covering the stretching sheet. In this segment, we inspect the physical outcomes of sundry parameters with respect to the velocity $f'(\eta)$, temperature $\theta(\eta)$ and species distribution $\phi(\eta)$. This segment contains the effects of dimensionless parameters like M, θ_w, Pr, Sc, Ec, σ, Rd, E which are demonstrated in Figs. 2, 3, 4, 5, 6, 7, 8 and 9. The outcomes are obtained for two diverse cases of CNT's, predominantly, SWCNT's and MWCNT's (blue coloured solid line denotes SWCNT's and green coloured dashed lines denotes MWCNT's) for blood flow. In Table 1, the numerical standards of CNT's and host fluid are revealed. The Prandtl number of blood is engaged as 21,and it behaves as non-Newtonian due to the existence of red blood cells. The variation of other parameters are constant, i.e., $M = 0.5$, $\lambda = 0.5$, $Nr = 0.5$, $\gamma = 0.1$, $Sc = 0.5$,

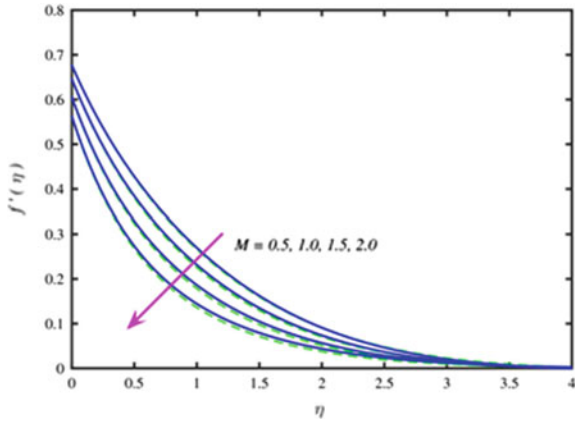

Fig. 2 M versus $f'(\eta)$

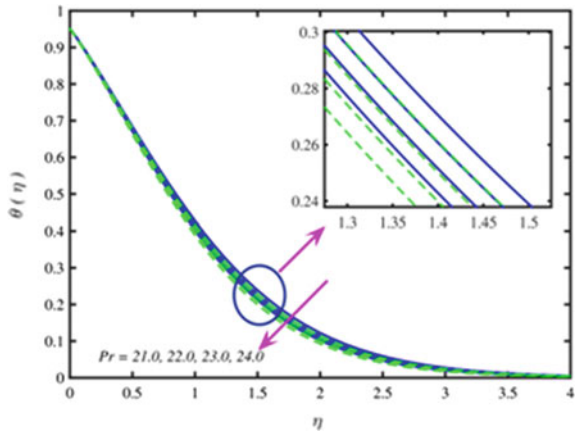

Fig. 3 Pr versus $\theta(\eta)$

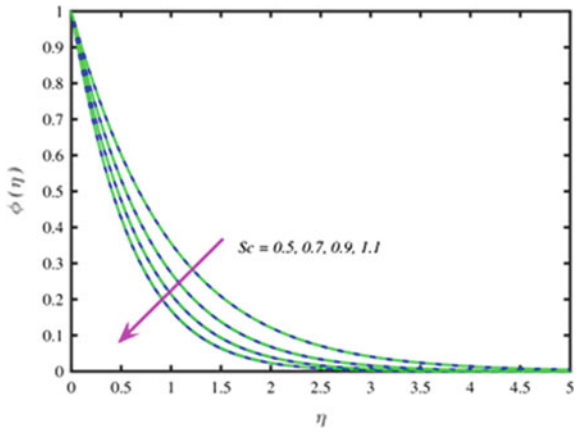

Fig. 4 *Sc* versus ϕ (η)

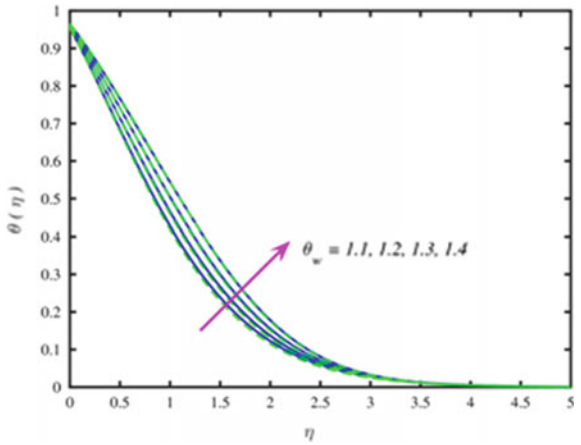

Fig. 5 θ_w versus θ (η)

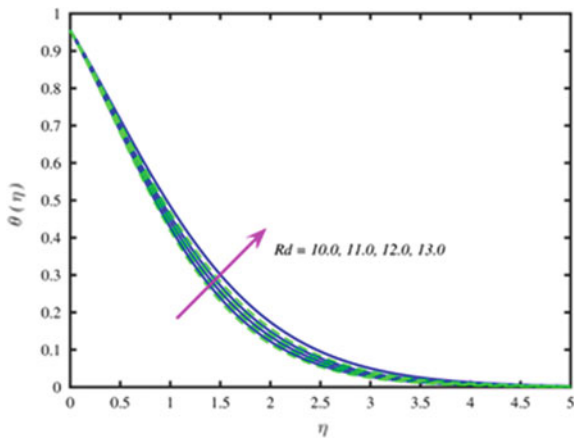

Fig. 6 Rd versus $\theta(\eta)$

Fig. 7 E versus $\phi(\eta)$

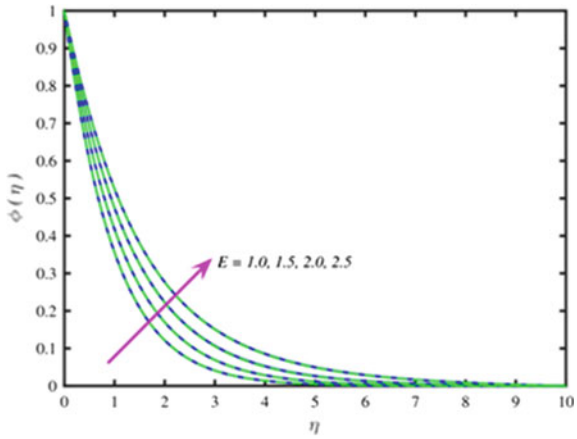

Fig. 8 Ec versus θ (η)

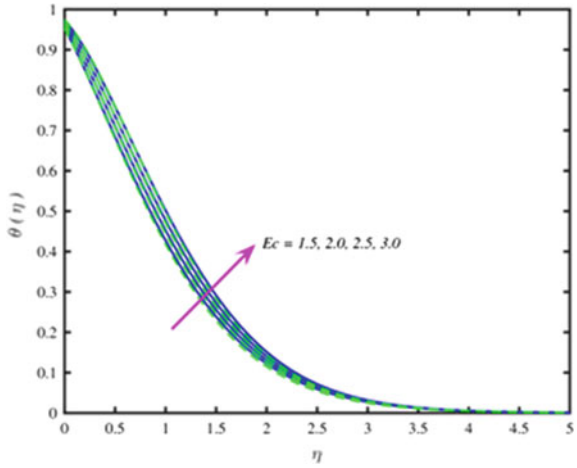

Fig. 9 σ versus $\phi(\eta)$

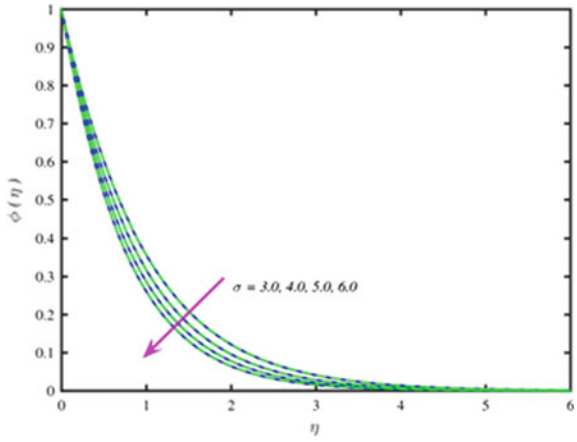

Ec = 1.5, $\theta_w = 1.1$, Bi = 10, $E = 1.0$, $\delta = 0.5$, $S = 0.5$, $A* = 0.05$, $B* = 0.05$, Rd = 10.0, $\sigma = 3.0$, $\chi = 0.06$, $\xi = \frac{\pi}{4}$, unless otherwise specified. Table 2 describes the deviations of skin friction for different parameters. The skin friction decreases with growing of M and ξ, and a reverse trend for Ec and χ. Table 3 displays the variations in rate of heat transfer for different values of M, Pr, Ec and χ. Heat transfer rate accelerates with Pr and decelerates with M, Ec and χ. Table 4 provides the sample values of mass transfer for several values of embedding parameters. Mass transfer declines for M, whereas it inclines with Sc, θ_w and χ. The upshot of M on velocity is perceived in Fig. 2. As M is grown, the velocity of the fluid diminishes (for both types of CNT's), and a decrease in the width of the velocity boundary layer is seen. Physically, a force called as Lorentz force opposes the movement and boosts up the molecules to collide. This force slows down the flow and is accountable in velocity decrement. Analysis of Pr on temperature is drafted in Fig. 3. Physically, the temperature and the width of the temperature boundary layer are counter in nature with

Table 2 Deviations in skin friction coefficient and various dimensionless parameters

M	Ec	χ	ξ	$f''(0)$	
				SWCNT	MWCNT
0.2	0.02	0.06	$\frac{\pi}{4}$	−0.6096	−0.6310
0.3	0.02	0.06	$\frac{\pi}{4}$	−0.6162	−0.6378
0.4	0.02	0.06	$\frac{\pi}{4}$	−0.6253	−0.6472
0.2	0.03	0.06	$\frac{\pi}{4}$	−0.6092	−0.6307
0.2	0.04	0.06	$\frac{\pi}{4}$	−0.6089	−0.6305
0.2	0.02	0.07	$\frac{\pi}{4}$	−0.5926	−0.6215
0.2	0.02	0.08	$\frac{\pi}{4}$	−0.5658	−0.6076
0.2	0.02	0.06	$\frac{\pi}{3}$	−0.6122	−0.6337
0.2	0.02	0.06	$\frac{\pi}{2}$	−0.6149	−0.6365

Table 3 Deviations in the rate of heat transfer and various dimensionless parameters

M	Pr	Ec	χ	$-\theta'(0)$	
				SWCNT	MWCNT
0.2	21.0	0.02	0.06	7.3704	8.0949
0.3	21.0	0.02	0.06	7.3513	8.0748
0.4	21.0	0.02	0.06	7.3253	8.0471
0.2	22.0	0.02	0.06	7.7201	8.4573
0.2	23.0	0.02	0.06	8.0652	8.8149
0.2	21.0	0.03	0.06	7.3468	8.0708
0.2	21.0	0.04	0.06	7.3232	8.0467
0.2	21.0	0.02	0.07	5.3761	6.6444
0.2	21.0	0.02	0.08	1.9658	4.4405

Table 4 Deviations in the rate of mass transfer and various dimensionless parameters

M	Sc	θ_w	χ	$-\phi'(0)$	
				SWCNT	MWCNT
0.2	0.6	1.1	0.06	1.1088	1.1067
0.3	0.6	1.1	0.06	1.1081	1.1059
0.4	0.6	1.1	0.06	1.1070	1.1048
0.2	0.7	1.1	0.06	1.2179	1.2155
0.2	0.8	1.1	0.06	1.3218	1.3192
0.2	0.6	1.2	0.06	1.1366	1.1340
0.2	0.6	1.3	0.06	1.1671	1.1641
0.2	0.6	1.1	0.07	1.1139	1.1107
0.2	0.6	1.1	0.08	1.1209	1.1156

Pr. The reduction in temperature profile for high Pr involves low heat conductivity which results in low fluid temperature for both SWCNT's and MWCNT's. As Sc is inversely associated with the mass diffusion coefficient D, as a result, larger values of Sc denote smaller D and for that leads to thinner concentration at the boundary layer. Thus, the nanoparticle concentration depreciates for both types of CNT's by the elevated values of Sc which is portrayed in Fig. 4. As values of θ_w mounts, a climb in temperature is seen in Fig. 5, and for that reason, growing θ_w results in elevation of wall temperature that successively yields a wider penetration depth for temperature when compared to ambient temperature, consequently fluid temperature enriches. Figure 6 depicts the impression of Rd on temperature and examined that the temperature inflates by raising the values of Rd. The reason behind is the mean absorption coefficient downwards for an upwards in Rd. In point of physics, at radiation, more heat absorbed by the working fluid consequently shows a rise in temperature. Further, the thickness of the thermal boundary layer was built up strongly by raising the values of non-linear radiation parameter. Activation energy E is plotted in Fig. 7 which is evident that as E enlarges the concentration would be larger. To initiate a larger chemical reaction, a huge amount of energy is needed. With the increasing values of E, the Arrhenius function decreases, and as a consequence, the chemical action raises the concentration. With more activation energy and less temperature, it results to a minor reaction rate that decelerates the chemical action. Therefore, the concentration of species increases. To explore the behaviour of Ec on the temperature profiles is plotted in Fig. 8. As Ec rises, the heat of the fluid also rises which leads to solidify the thermal boundary layer which is constant with heat generation due to the frictional property of the fluid. The heat generated by viscous dissipation owed to haul among the fluid particles, and this additional heat results an enhancement in temperature of the initial fluid for both single- and multi-walled CNT's. Figure 9 depicts the impact of reaction rate constant σ on concentration. When we gradually increase σ, the concentration becomes thin out. A favourable destructive reaction rises which consecutively results in a fall in concentration. Due to this concentration,

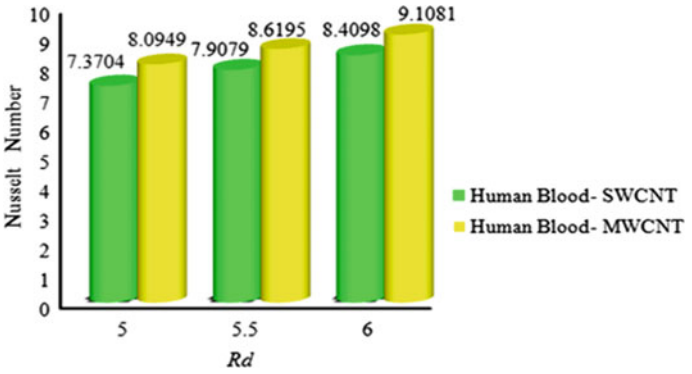

Fig. 10 *Rd* versus Nusselt number

profile decreases, and same consequence is seen for both CNT's. Figure 10 illustrates the variation in local Nusselt number for different values of non-linear thermal radiation. It is clear that escalating values of Rd improves the heat transformation rate for both cases. The enhancement for MWCNT's is slightly more when compared with SWCNT's. The effect of θ_w on local Nusselt number is demonstrated in Fig. 11 and is detected that rising values of θ_w raises the local Nusselt number for both circumstances. The effect of A^* and B^* on local Nusselt number is demonstrated in Figs. 12 and 13. It is noted that rising values of A^* and B^* fall the local Nusselt number for both SWCNT's and MWCNT's. The increment for MWCNT's is more than with SWCNT's. Figure 14 exemplifies the effect of Sherwood number on chemical reaction rate constant. The outcomes show a rise in σ which raises Sherwood number for both SWCNT's and MWCNT's. Figure 15 exemplifies the effect of Sherwood number on Activation Energy. The figure shows a rise in E which has a fall in the Sherwood number for both conditions.

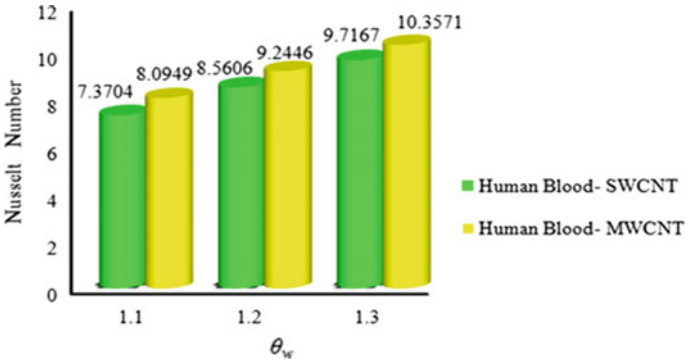

Fig. 11 θ_w versus Nusselt number

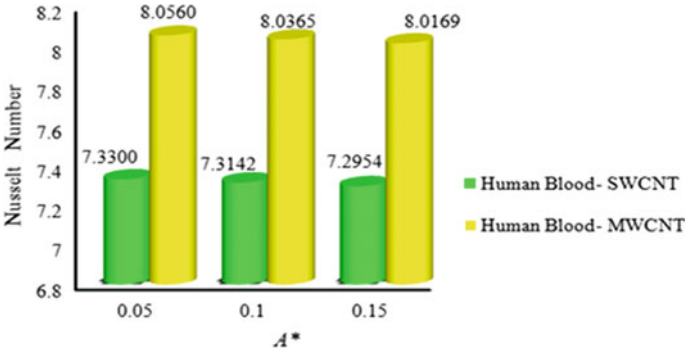

Fig. 12 A^* versus Nusselt number

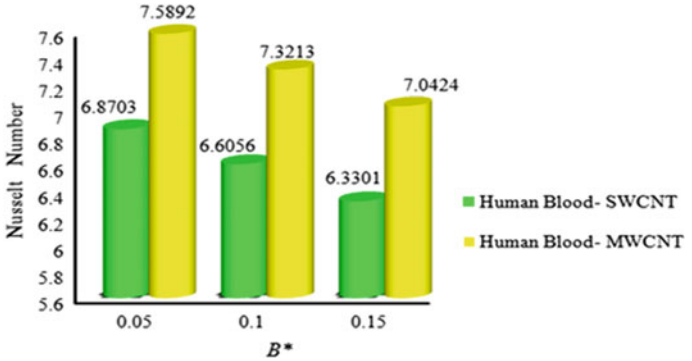

Fig. 13 B^* versus Nusselt number

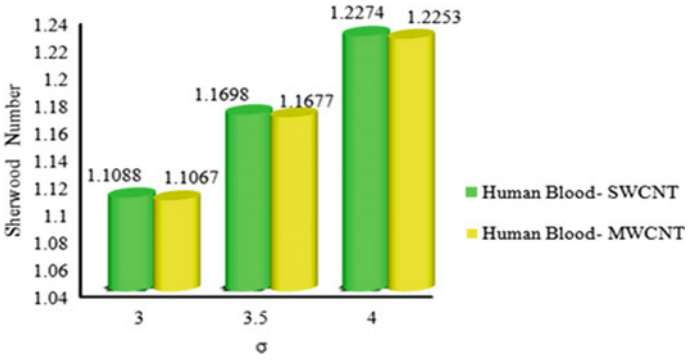

Fig. 14 σ versus Sherwood number

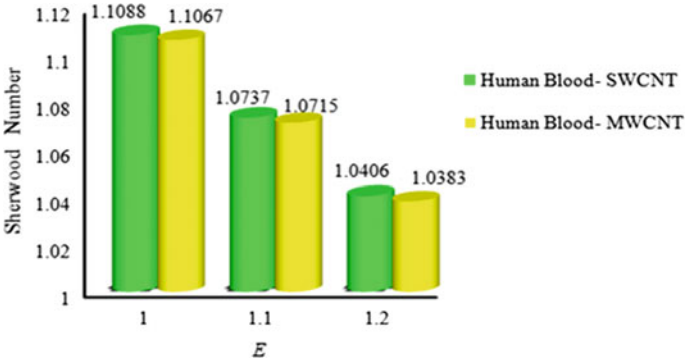

Fig. 15 E versus Sherwood number

5 Final Conclusions

The current communication scrutinizes a theoretical model of blood with carbon nanotubes (CNT's)—ejected in a Maxwell fluid with nanoparticles through binary chemical reaction lying on a stretching sheet by means of aligned magnetic field. The strategic upshots of this framework are outlined below

- Increasing values of Rd,θ_w, Ec *and* χ, lead to stronger temperature distribution.
- The higher value of Sc, reaction rate parameter and concentration decreases.
- The fluid concentration rises with E.
- A rise in σ raises Sherwood number.
- A rise in E has a fall in the Sherwood number.

References

1. Baughman RH, Zakhidov AA, De Heer WA (2002) Carbon nanotubes-the route toward applications. Science 297(5582):787–792. https://doi.org/10.1126/science.1060928
2. Cattaneo C (1948) Sulla conduzionedelcalore, AttiSemin. Mat Fis Univ Modena Reggio Emilia 3:83–101
3. Christov CI (2009) On frame indifferent formulation of the Maxwell-Cattaneo model of finite speed heat conduction. Mech Res Commun 36:481–486. https://doi.org/10.1016/j.mechrescom.2008.11.003
4. Bala Anki Reddy P, Suneetha S (2018) Impact of Cattaneo-Christov heat flux in the Casson fluid flow over a stretching surface with aligned magnentic field and homogeneous heterogeneous chemical reaction. Front Heat Mass Transfer 10(7). https://doi.org/10.5098/hmt.10.7
5. Kolin (1936) Electromagnetic flow meter: principle of method and its applications to blood flow measurement. In: Proceedings of the society for experimental biology and medicine, vol. 35, pp. 53–56

6. Sinha A, Misra JC, Shit GC (2016) Effect of heat transfer on unsteady MHD flow of blood in a permeable vessel in the presence of non-uniform heat source. Alexandria Eng J 55(3):2023–2033. https://doi.org/10.1016/j.aej.2016.07.010
7. Sud VK, Sekhon GS (1989) Blood flow through the human arterial system in the presence of a steady magnetic field. Physiol Med Biol 34(7):795–805
8. Szasz A (2007) Hyperthermia, a modality in the wings. J Cancer Res Ther 3(1):56–66
9. Shehzad SA, Hayat T, Alsaedi A, Obid MA (2014) Nonlinear thermal radiation in three-dimensional flow of Jeffrey nanofluid: a model for solar energy. Appl Math Comput 248:273–286. https://doi.org/10.1016/j.amc.2014.09.091
10. Hayat T, Imtiaz M, Alsaedi A, Kutbi MA (2015) MHD three-dimensional flow of nanofluid with velocity slip and nonlinear thermal radiation. J Magn Magn Mater 396:31–37. https://doi.org/10.1016/j.jmmm.2015.07.091
11. Hayat T, Muhammad T, Alsaedi A, Alhuthali M (2015) Magnetohydrodynamic three-dimensional flow of viscoelastic nanofluid in the presence of nonlinear thermal radiation. J Magn Magn Mater 385:222–229. https://doi.org/10.1016/j.jmmm.2015.02.046
12. Bala Anki Reddy P, Suneetha S, Bhaskar Reddy N (2017) Numerical study of MHD Boundary Layer Slip Flow of a Maxwell Nanofluid over an exponentially stretching surface with convective boundary condition. Propulsion Power Res **6**(4):259–268 (2017). https://doi.org/10.1016/j.jppr.2017.11.002
13. Misra JC, Kar BM (1989) Momentum integral method for studying flow characteristics of blood through a stenosed vessel. Biorheology **26**(1):23–25 (1989). https://doi.org/10.3233/BIR-1989-26102
14. Gebhart B (1962) Effects of viscous dissipation in natural convection. J Fluid Mech 14(2):225–232. https://doi.org/10.1017/S0022112062001196
15. Reddy SRR, Bala Anki Reddy P, Suneetha S (2018) Magneto hydro dynamic flow of blood in a permeable inclined stretching viscous dissipation, non-uniform heat source/sink and chemical reaction. Front Heat Mass Transfer 10(22). https://doi.org/10.5098/hmt.10.22
16. Gireesha BJ, Mahanthesh B, Rashidi MM (2015) MHD boundary layer heat and mass transfer of a chemically reacting Casson fluid over a permeable stretching surface with non-uniform heat source/sink. Int J Indus Math 7(3):247–260
17. Mabood F, Ibrahim SM, Rashidi MM, Shadloo MS, Lorenzini G (2016) Non-uniform heat source/sink and Soret effects on MHD non-Darcian convective flow past a stretching sheet in a micropolar fluid with radiation. Int J Heat Mass Transf 93:674–682. https://doi.org/10.1016/j.ijheatmasstransfer.2015.10.014
18. Ali N, Ullah Khan S, Sajid M, Abbas Z (2016) MHD flow and heat transfer of couple stress fluid over an oscillatory stretching sheet with heat source/sink in porous medium. Alexandria Eng J 55(2):915–924. https://doi.org/10.1016/j.aej.2016.02.018
19. Srinivas S, Reddy PBA, Prasad BSRV (2014) Effects of chemical reaction and thermal radiation on MHD flow over an inclined permeable stretching surface with non-uniform heat source/sink: an application to the dynamics of blood flow. J Mech Med Boil 14(5):1450067. https://doi.org/10.1142/S0219519414500675
20. Mohammadein SA, Raslan K, Abdel-Wahed MS, Abedel-Aal Elsayed M (2018) KKL-model of MHD CuO-nanofluid flow over a stagnation point stretching sheet with nonlinear thermal radiation and suction/injection. Results Phys 10:194–199. https://doi.org/10.1016/j.rinp.2018.05.032
21. Bestman AR (1990) Natural convection boundary layer with suction and mass transfer in a porous medium. Int J Eng Res 14:389–96
22. Shafique Z, Mustafa M, Mushtaq A (2016) Boundary layer flow of Maxwell fluid in rotating frame with binary chemical reaction and activation energy. Results Phys 6:627–633. https://doi.org/10.1016/j.rinp.2016.09.006
23. Lu D, Ramzan M, Ahmad S, Dong Chung J, Farooq U (2017) Upshot of binary chemical reaction and activation energy on carbon nanotubes with Cattaneo-Christov heat flux and buoyancy effects. Phys Fluids 29:123103 (2017)

24. Dhlamini M, Kameswaran PK, Sibanda P, Motsa S, Mondal H (2018) Activation energy and binary chemical reaction effects in mixed convective nanofluid flow with convective boundary conditions. J Comput Design Eng 6:149–158. https://doi.org/10.1016/j.jcde.2018.07.002
25. Khalid A, Khana I, Khan A, Shafied S, Tlilie I (2018) Case study of MHD blood flow in a porous medium with CNTS and thermal analysis. Case Stud Thermal Eng 12:374–380. https://doi.org/10.1016/j.csite.2018.04.004